Type of contribution:
Editorial
▶ Research Paper
Case Study
Review Paper
Scientific Data
Report of Tech. Application

e-issn. 2798-5245

Mechanical Engineering for Society and Industry
Vol. 5, No. 1 (2025) pp 133-144
https://doi.org/10.31603/mesi.12913

Development of hybrid nanofluids and solar heat exchangers (SHX) to improve heat transfer performance in solar panel cooling

Amri Abdulah[1]*, Apang Djafar Shieddique[1], Dede Ardi Rajab[1], Khoirudin[2], Sukarman[2]*

[1] Department of Mechanical Engineering, Sekolah Tinggi Teknologi Wastukancana, Purwakarta 41151, **Indonesia**
[2] Department of Mechanical Engineering, Universitas Buana Perjuangan, Karawang 41361, **Indonesia**
✉ amri@wastukancana.ac.id

Highlights:

- A solar heat exchanger (SHX) design was successfully created and proven to be effective.
- Hybrid nanofluid Al_2O_3+ SiO_2+EG/W (10:90) can increase cooling performance up to 56.07%.
- The effectiveness of the Al_2O_3+SiO_2+EG/W (10:90) hybrid nanofluid for SHX was 117%.
- The calculation and experimental accuracies were quite accurate; through the uncertainty analysis of the Nusselt number, the value was 0.26%, whereas the Reynolds number was 1.7%.

Abstract

This study examined the thermohydraulic efficiency of a novel Solar Heat Exchanger (SHX) designed for cooling solar panels. The SHX was specifically created for 20 Wp solar panels measuring 450 × 350 mm. The cooling medium was a hybrid nanofluid (HNF) consisting of Al_2O_3 and SiO_2 nanoparticles (0.5–1%) suspended in a base fluid of ethylene glycol and water (EG/W) at a 10:90 ratio. Experiments were performed using flow rates ranging from 1 to 3 LPM. The HNF coolant demonstrated enhanced performance in the solar heat exchanger, with a maximum heat transfer rate increase of 56.07% compared with that of the base fluid. This improvement in the heat-transfer rate was associated with an increase in the heat-transfer coefficient, which was influenced by the flow rate and volume fraction of the HNF. The effectiveness of the HNF surpassed that of the base fluids by approximately 117%. The results indicated that higher flow rates and volume fractions improved cooling performance. The enhanced cooling efficiency and innovative SHX design make this study particularly relevant to the development of solar panel cooling systems, particularly those employing hybrid nanofluid coolants.

Keywords: Hybrid nanofluids; Solar Heat Exchanger; Thermal conductivity; Al_2O_3; SiO_2

Article info
Submitted: 2024-12-28
Revised: 2025-02-27
Accepted: 2025-03-09

Publisher
Universitas Muhammadiyah Magelang

1. Introduction

In recent years, solar-panel cooling has become a topic of interest. The reduction in the surface temperature of solar cells is carried out from various perspectives, such as the type of

Nomenclature			
NP	Nanoparticle, (–)	SHX	Solar heat exchanger, (–)
NF	Nanofluid, (–)	SSA	Surface specific Area, (m^2/g)
HNF	Hybrid nanofluid	MNF	Mono nanofluid
TC	Thermal conductivity, (W/m.K)	PV	Photo voltaik
HTC	Heat transfer coefficient	CoA	Certificate of analysis
EG/W	Ethylene glycol water mixture, (–)	LPM	Liter per minute
ρ	Density, (kg/m^3)	T_b	Bulk temperature, (C)
φ	Volume concentration, (%)	T_w	Wall temperature, (C)
Cp	Specific heat, (J/kg.K)	Q	Heat transfer rate, (Watt)
μ	Viscosity, (mPa.s)	D_h	Hydraulic diameter, (mm)
k	Thermal conductivity, (W/m.K)	h	Heat transfer coefficient
nf	Nanofluid, (–)	p	Circumference, (m)
f	Base fluid, (–)	As	Cross sectional area, (m^2)
bf	Base fluid, (–)	R_{th}	Thermal resistance, (–)
v	Velocity, (m/s)	η_{th}	Thermal effectiveness, (–)
m	Mass flow rate, (kg/s)	P	Pressure, (Bar)
T_i	Inlet temperature, (C)	Nu	Nusselt number, (–)
T_o	Outlet temperature, (C)	Re	Reynolds number, (–)

coolant using air [1], [2], [3] and liquid, and the design of the thermal collector [4]. According to Huang *et al.* [5], when the temperature exceeds a predetermined threshold and other environmental factors, such as wind direction and speed, the short-circuit current and open-circuit voltage of solar cells pose a significant risk to the output power of photovoltaic (PV) modules. From the fluid side, conventional coolants [6], phase-change materials-PV [7], [8], and nanofluids [9], [10], [11] are used as solar panel cooling media to improve the thermal performance, increase the electrical efficiency, make it durable, and prevent damage to solar cells. Recently, Hybrid nanofluids (HNF), which are an advanced engineering of mono-nanofluids, are believed to have better transfer performance owing to the high kinetic energy generated by nanoparticle collisions [12], [13].

Nanofluids (NF) for solar panel cooling with several types of nanoparticles (NP), such as carbon-coated cobalt [14], SiC [15], TiO_2 [16], and Al_2O_3 [17], [18], [19], [20], exhibit good performance in improving fluid performance. Al-Waeli *et al.* [15] added 3 wt.% SiC into water resulting in an increase in thermal conductivity (TC) of up to 8.2%. The efficiency increased by 24.12%, and the panel surface temperature decreased by 16 °C. Murtadha *et al.* [16] conducted a study using TiO_2 mono nanofluid (MNF) with a concentration of 1-3 wt%. The results showed that the highest concentration exhibited the highest efficiency (19.23%). Fikri *et al.* [21] also used TiO_2 and mixed it with SiO_2 nanoparticles at ratios of 30:70 and 70:30 to form HNF. Their results showed that the highest TC of the TiO_2- SiO_2 HNF was produced at a ratio of 30:70. Azmi *et al.* [22] also used TiO_2-SiO_2 HNF and the heat transfer of TiO_2- SiO_2 HNF was enhanced up to 211.75%. Furthermore, Ramadhan [23] Azmi and developed tri-hybrid nanofluids (Al_2O_3-TiO_2-SiO_2) and found that Al_2O_3-TiO_2-SiO_2 nanofluids with a mixing ratio (20:64:16) exhibited the lowest relative viscosity.The same NP mixture was also used in radiator applications by Ramadhan *et al.* [24] and resulted in a maximum increase in the heat transfer coefficient (HTC) for the air side observed up to 23.8% at a volume concentration of 0.05%. Studies have revealed that Al_2O_3 is widely used in nanofluids owing to its advantages in terms of fluid thermal properties. Al_2O_3 is abundant and easy to obtain [17].

Nanoparticles (NP) for nanocoolants are selected based on their thermophysical properties, such as alumina (Al_2O_3), which is a good insulator or heat and electricity barrier and has a high TC. Water and Ethylene Glycol are commonly used as base fluids in heat exchangers. Despite their poor conductivities, EG/water (EG/W) base fluids are widely used to prepare nanofluids, and a certain ratio is used to overcome the low boiling point of water [25]. Further developments in base fluids, namely the use of EG/water-based base fluids, have received much attention, perhaps because they have good heat-transfer characteristics, particularly in cold climates [26], as performed by Sundar et al. [18], to increase the TC of the combination of Al_2O_3 and three variations of EG/W, namely, the 80:20, 60:40, and 40:60 ratios. Vajjha and Das [19] also used EG fluid. Esfe *et al.* [20] conducted a study on the TC of Al_2O_3 mixed with EG/W at a ratio of 60:40.

This study presents a novel approach utilizing hybrid nanofluids (HNF) composed of SiO_2 and Al_2O_3 (30:70 ratio) dispersed in an EG/W base fluid with a 10:90 ratio. Unlike previous research, which focused on limited volume fractions (0.5–1 vol. %, %) and particle sizes of 30 nm and 50 nm for SiO_2 and Al_2O_3, respectively, this study explores a broader range of volume fraction variations to identify optimal parameters for enhancing heat transfer performance. The innovation of this study lies in the experimental investigation of the thermal performance of HNF in an SHX specifically designed for solar-panel cooling applications. The SHX features a tortuous channel configuration tailored to the surface contour and dimensions of a 20 Wp solar panel (315×450×15 mm). This customized design ensures efficient heat dissipation while maintaining compatibility with the physical characteristics of the solar panel. Additionally, this study examined the impact of significant variations in HNF flow rates, ranging from 1 to 3 LPM, to systematically evaluate their influence on heat transfer performance. The primary objective of this study was to investigate the synergistic effects of the volume fraction and flow rate on the thermohydraulic performance of HNF in solar panel cooling systems. By addressing these factors, this study aims to fill critical knowledge gaps, advance the understanding of HNF behavior under varying operational conditions, and provide a practical foundation for developing more efficient and sustainable cooling solutions for photovoltaic systems.

2. Materials and methods

2.1. Preparation of HNF coolant

Alumina was sourced from suppliers in Hebei Province, China. The alumina measured 50 nm with a purity level of 99.99%, whereas the average size of the silica was 30 nm. The base liquid for these HNF was a mixture of ethylene glycol (EG) and water (EG/W). The HNF was prepared using a two-step method: the process began by mixing the EG/W 10:90 base liquid. Following the mixing process, the base fluid was subjected to magnetic stirring (Cimarec, Thermo Fisher Scientific) for 1 h to ensure a homogeneous distribution. Upon completion of the base fluid stirring process, Al_2O_3 and SiO_2 in a 70:30 ratio were introduced into the base fluid, followed by an additional hour of magnetic stirring. The mixture was then sonicated for 1 h using an ultrasonicator (DAIHAN Scientific).

Table 1. Thermophysical properties of the base fluid EG/W (10:90) at 30 °C [25]

Parameter	Value
Density, ρ (kg/m3)	1009.92
Specific heat, Cp (J/kg.K)	3989
Viscosity, μ (mPa.s)	0.97
Thermal conductivity, k (W/m.K)	0.556

Table 2. Thermophysical properties of Al_2O_3 and SiO_2 NPs

Properties	Al_2O_3	SiO_2	Ref
Size (nm)	50	30	CoA
Purity (%)	99.9	99.8	CoA
pH Value	6–9	7–8	CoA
SSA (m^2/g)	100–160	150–300	CoA
Density, ρ (kg/m^3)	4000	2200	[27]
Specific heat, *Cp* (J/kg.K)	773	745	[27]
Thermal conductivity, *k* (W/m.K)	36	1.4	[27]

EG has the advantage of a high boiling point of ≥ 195 °C [25]; therefore, it is widely used for coolant mixtures. The specifications of the EG are listed in **Table 1**. The NP specifications obtained from the analysis certificate used in this study are listed in **Table 2**. The thermophysical properties of HNF are important factors for improving their performance, and thermophysical properties, such as heat capacity and mass density, were estimated based on Eq. (1) and (2), respectively [28].

$$\rho_{nf} = \varphi\rho_p + (1-\varphi)\rho_f \tag{1}$$

$$C_{nf} = (1-\varphi)\left(\frac{\rho_f}{\rho_{nf}}\right)Cp_f + \varphi\left(\frac{\rho_p}{\rho_{nf}}\right)Cp_p \tag{2}$$

Viscosity was calculated using Eq. (3) [29].

$$\mu_{nf} = \mu_f(1+2.5\varphi) \tag{3}$$

TC was predicted using Eq. (4) from Hamilton−Crosser [30].

$$\frac{k_{nf}}{k_f} = \frac{k_p + (n-1)k_f - (n-1)\left(k_f - k_p\right)\varphi}{k_p + (n-1)k_f - \left(k_f - k_p\right)\varphi} \tag{4}$$

where *k* is the thermal conductivity, *p* is the nanoparticle, *nf* is the nanofluid, φ is the volume fraction, *f* is the basic fluid, and *n* is the shape factor. In addition to being calculated, the viscosity and TC were measured using a TC analyzer and viscosity tester. The equipment used is illustrated in **Figure 1**.

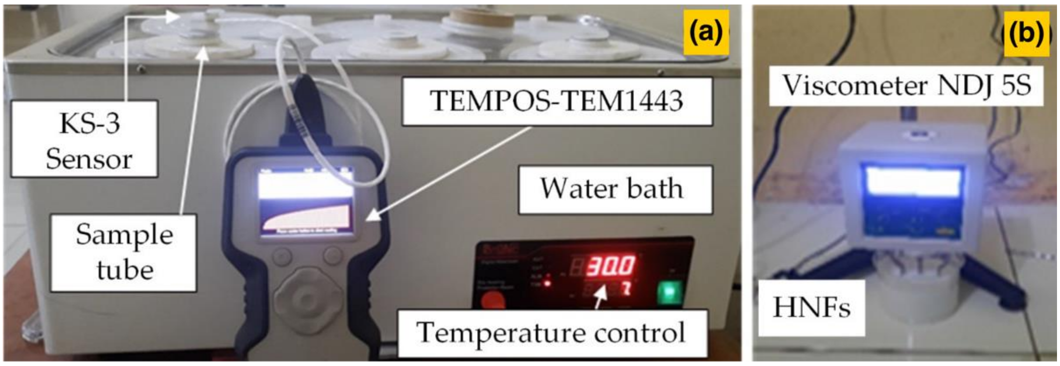

Figure 1. Experimental setup for thermophysical property measurements: (a) Thermal conductivity (TC) analyzer; (b) Viscometer for viscosity measurement

2.2. Design of Solar Heat Exchanger (SHX)

Testing on experimental test equipment for forced convection heat transfer was carried out with variations in the percentage of NP, ϕ = 0.5–1 vol. % and EG/water (10:90) and variations in volumetric flow rate and HNF temperature. The obtained data included the temperature in the SHX of the solar-panel cooling system. Furthermore, the data obtained from the test, namely, the temperature, fluid flow rate, heat transport, and fluid pressure in the SHX for PV cooling using HNF, were analyzed. The complete design of the SHX is illustrated in **Figure 2**.

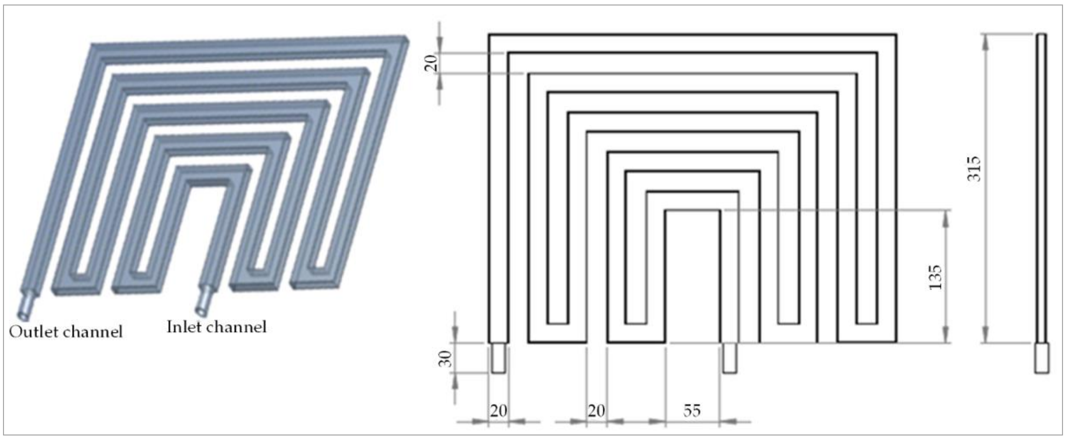

Figure 2. Schematic representation of the solar heat exchanger (SHX) design

Figure 2 shows the design of the SHX, which features a compact U-shaped coiled-tube configuration. The system was made of stainless steel with dimensions of 20 mm in width, 10 mm in height, and a wall thickness of 1.2 mm. This design enhances the heat transfer efficiency while maintaining structural durability under varying thermal loads. The coiled layout ensures optimal fluid flow distribution, promoting effective heat exchange. The overall dimensions included a total width of 315 mm and length of 450 mm, with tubes precisely spaced to achieve uniform heat absorption. This design is particularly suitable for 20 Wp solar thermal applications that require efficient energy transfer. A similar system was used by Prasetyo *et al.* [4], but it differed in terms of the total size, which was 480 × 570 mm with a hollow dimension of 30 × 30 mm, whereas the current study had a total size of 315 × 450 mm with a hollow section size of 10 × 20 mm.

A schematic of the closed-loop setup of the experimental equipment for PV cooling is shown in **Figure 3**. The closed loop consists of several main components: a solar heat exchanger (SHX), pump, refrigerant cooler, and reservoir. A circulation pump (model RGZB8/15) was used to push the HNF through the SHX, where the HNF became hot after absorbing heat from the heat source. To recirculate, the HNF must be cold when entering the SHX. The condensation process uses a refrigerant cooler with a coil-shaped refrigerant pipe wrapped around the cooler reservoir. The hot HNF was cooled in the reservoir and was ready to be recirculated to the same process through the system. A rectangular SHX with dimensions of 350 mm × 450 mm was fabricated using hollow stainless steel, and a detailed image of the channel is shown in **Figure 3**. Each channel was spaced 20 mm apart and had a height of 10 mm. A 650 W cartridge heater was positioned on the bottom plate directly below the SHX to simulate the heat generated by the solar panels. The temperature of the system was measured using a K-type thermocouple. One thermocouple was used to control the heat generated by the cartridge heater, and the other three thermocouples were used to measure the bottom surface temperature (Twall) of the SHX. The temperature data in the experiment were determined by calculating the average values of the three thermocouples at dif-

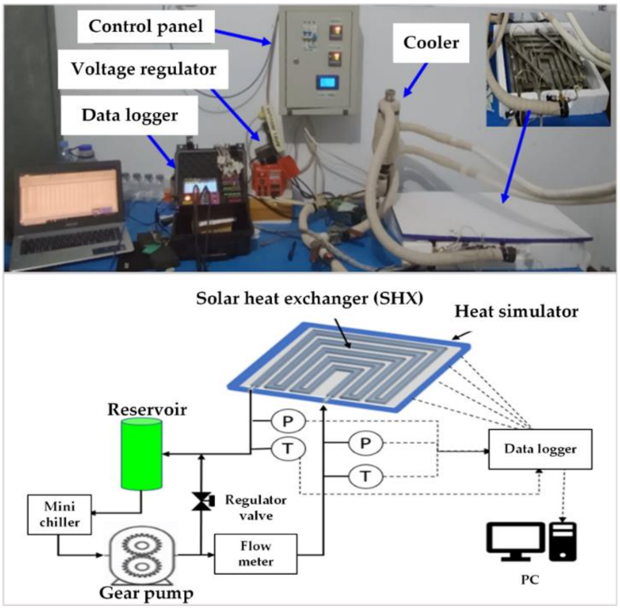

Figure 3. Experimental setup for performance testing of the solar heat exchanger (SHX)

ferent positions. The SHX was placed in an insulated box to ensure maximum heat absorption. The temperature of the fluid passing through the SHX was measured using two temperature sensors. Flow meters and pressure transducers were installed to measure the pressure drop in the SHX and the flow rate. All the data from the experimental tests were recorded using a data logger.

2.3. Heat Transfer Reduction Data

The law of conservation of energy for the fluid flow in a fixed channel is expressed by Eq. (5), where T_i and T_o inlet and outlet temperatures of the SHX, respectively; $\dot{Q}$ is the heat transfer rate; *and m* and *Cp* are the mass flow rate and heat capacity, respectively. SHX undergoes forced convection heat transfer (*h*); therefore, Eq. (8) was used to obtain the convection coefficient. The heat transport efficiency is influenced by the coolant entry and exit temperatures, as well as the SHX base temperature. Consequently, the log mean temperature difference (ΔT_{lmtd}) technique is an appropriate method for evaluating the thermal performance of heat exchanger. In this study, ΔT_{lmtd} was determined using Eq. (6), which considers the base temperature of the SHX.

$$Q = m\ Cp\ (T_{i-}T_o) \tag{5}$$

$$\Delta T_{lmtd} = \frac{(T_b - T_{i.hnf}) - (T_b - T_{o.hnf})}{ln\dfrac{(T_b - T_{i.hnf})}{(T_b - T_{o.hnf})}} \tag{6}$$

$$D_h = 4A_s/p \tag{7}$$

$$h = \frac{Q}{(\Delta T_{lmtd})A_s} \tag{8}$$

where A_s is the cross-sectional area of the rectangular pipe, *p* is its circumference, *h* is the heat transfer coefficient, *and* T_b is the bulk temperature ($T_b = (T_i - T_o) / 2$). For a pipe with a rectangular hollow section, *Dh* can be expressed as follows (Eq. (7)): the heat removal efficiency of the coolant is hindered by the thermal resistance. Eq. (9) can be used to determine the resistance encountered by the HNF fluid during the flow.

$$R_{th} = \frac{1}{hA_s} = \frac{\Delta T_{lmtd}}{q_{hnf}} \tag{9}$$

The thermal effectiveness of SHX, based on the higher wall temperature (*Tw.max*), was estimated using Eq. (10).

$$\eta_{th} = 1 - \frac{(T_{w.max} - T_{in})_{hnf}}{(T_{w.max} - T_{in})_{bf}} \tag{10}$$

The pumping power caused by the pressure drop was estimated using Eq. (11):

$$P_p = Q\ \Delta P \tag{11}$$

2.4. Uncertainty Analysis

The TC in this study was tested experimentally, and its value affected the Nusselt and Reynolds numbers. The uncertainty of the Nusselt number was analyzed using Eq. (12) [31] and the Reynolds number was analized using Eq. (13) [32].

$$\frac{\delta Nu}{Nu} = \left[\left(\frac{\delta k}{k}\right)^2 + \left(\frac{\delta D_h}{D_h}\right)^2 + \left(\frac{\delta h}{h}\right)^2\right]^{1/2} \tag{12}$$

$$u^2(Re) = \left(\frac{\delta Re}{\delta \rho}\right)^2 u^2(\rho) + \left(\frac{\delta Re}{\delta v}\right)^2 u^2(v) + \left(\frac{\delta Re}{\delta D_h}\right)^2 u^2(D_h) + \left(\frac{\delta Re}{\delta \mu}\right)^2 u^2(\mu) \tag{13}$$

3. Results and Discussion

3.1. Termophsycal Properties

The thermophysical properties, such as density, calculated using Eq. (1), were in the range of ±1022–1034 kg/m³, whereas the heat capacity obtained using Eq. (2) was within ±3881–3994 J/kg. K. The viscosity, determined using Eq. (3), and TC derived from Eq. (4)are listed in **Table 3**. TC and viscosity measurements were performed using the test equipment shown in **Figure 1**. The results were compared for further analysis. The difference between the two results was not significant after the uncertainty analysis was performed using Eq. (12) and Eq. (13). Viscosity uncertainty analysis using Eq. (12) yielded a value of 0.26%. The TC uncertainty analysis using Eq. (13) yielded a 1.7%. These properties are essential for evaluating the heat-transfer performance of the HNF and serve as fundamental parameters in the heat-transfer analysis performed in this study.

The thermophysical properties calculated in this study provide a robust foundation for assessing the heat-transfer performance of HNF in SHX experiments. The interplay between these properties, particularly TC and viscosity, plays a critical role in determining the efficiency of heat transfer enhancement. A comprehensive comparison of these properties with literature values and experimental findings is summarized in **Table 3**.

Table 3. Thermophysical properties of hybrid nanofluids (HNF) at 30 °C

Thermal properties	0.5 vol.%	0.75 vol.%	1 vol.%
Density, ρ (kg/m³)	1022.1	1028.3	1034.4
Specific heat, *Cp* (J/kg.K)	3934.5	3907.8	3881.4
Viscosity, μ (kg/m.s)	0.000982	0.000988	0.000994
Thermal conductivity, k (W/mK)	0.618	0.6210	0.6235

Several previous investigations have reported similar trends in the thermophysical properties of nanofluids, particularly in HNF formulations. Khalid *et al.* [33] observed that the addition of Al_2O_3 and SiO_2 nanoparticles to water-based nanofluids significantly enhanced the TC while slightly increasing the viscosity, which is consistent with the results of this study. Similarly, Moldoveanu *et al.* [34] demonstrated that the TC of HNF exhibits a linear increase with volume fraction, influenced by Brownian motion and NP clustering effects.

3.2. Heat transfer in SHX

The thermal performance of the HNF depended on the convective heat coefficient, which was reflected by the values of the flow rate and volume fraction of the NP against the coefficient (*h*), as shown in **Figure 4**. The improved cooling efficiency and innovative SHX design make this study highly relevant to advanced solar panel cooling systems, particularly those that use HNF coolants.

The heat transfer coefficient was calculated using Eq. (8) based on the average heat transfer rate and mean log temperature difference. **Figure 4** emphasizes that there is an increase in the coefficient at a flow rate of 1–3 LPM with an increase in the volume fraction of NP from 0.5 to 1 vol.%, as illustrated in **Figure 5**. The rise in the Nusselt number is evident from calculations involving the coefficient, hydraulic diameter, and thermal conductivity (TC) of the hybrid nanofluid (HNF). The increase in nanoparticle (NP) volume fraction within the base fluid, along with Brownian motion, plays a significant role in enhancing the TC, which together contribute to the superior thermal performance of the HNF compared to the base fluid [35], [36]. Furthermore, an increase in flow rate leads to improved convective heat transfer in the cooler, resulting in the greatest reduction in the SHX base temperature. At the highest volume fraction tested, the HNF achieved a maximum increase of about 53%, surpassing the convective heat transfer coefficient of the base fluid. The enhanced thermal properties of the HNF relative to the base fluid are key to its improved convective performance. Heat transfer within fluid systems is influenced by multiple factors, notably the fluid flow rate and the NP concentration in the HNF. To analyze these effects, experiments were conducted by varying the HNF flow rate across different volume fractions (ϕ).

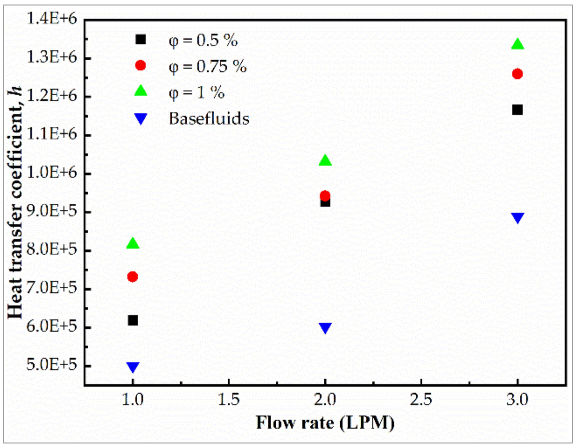

Figure 4. Variation of heat transfer coefficient (h) with different nanofluid concentrations

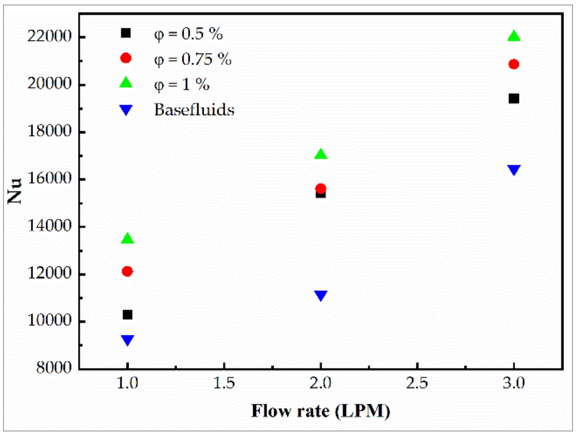

Figure 5. Effect of flow rate on the Nusselt number at varying nanofluid concentrations

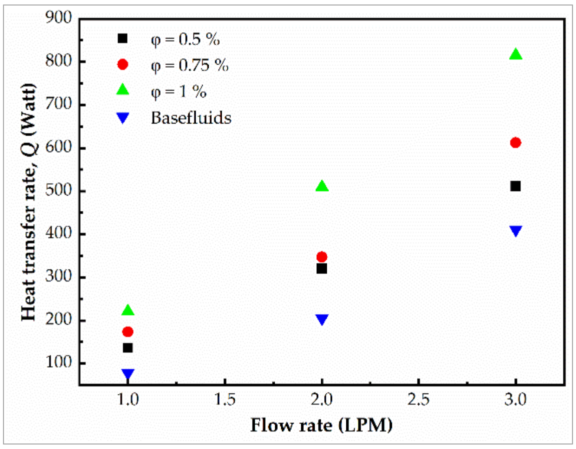

Figure 6. Effect of flow rate on heat transfer rate for different nanofluid concentrations

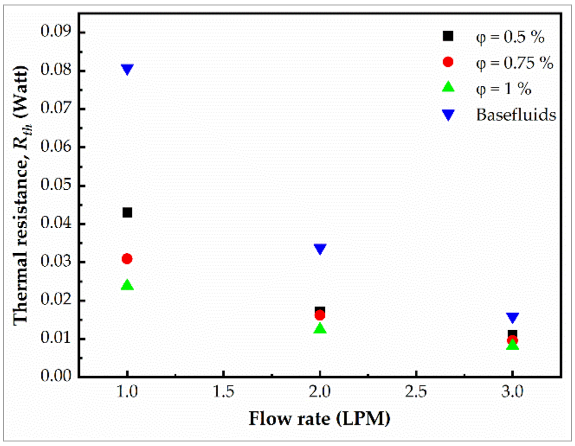

Figure 7. Effect of flow rate on thermal resistance at various nanofluid concentrations

Figure 6 shows the relationship between the fluid flow rate and heat transfer rate for HNF with volume fractions of 0.5, 0.75, and 1 vol. %, as well as for the base fluid. From the graph, increasing the flow rate increased the heat transfer rate for all samples. In addition, nanofluids with higher NP concentrations showed a more significant increase in the heat transfer rate than the base fluid, indicating the role of NP in improving heat transfer efficiency. The experimental results, shown in Figure 6, in the flow rate range of 1–3 LPM indicate that the HNF, with increasing volume fraction and flow rate, has a significant effect that ultimately reduces the temperature of the SHX base section. An increase in the heat transfer rate was observed at flow rates of 1–3 LPM, with a maximum increase of 56.07% when using HNF compared with the base fluid. This is in line with the report by Al-waeli *et al.* [15] which reported that utilizing 3 wt.% SiC reduced PV temperature by 16 °C and increased efficiency by 24.12%. As shown in Figure 6, the HNF demonstrated superior heat absorption compared to the base fluid, and an increase in the volume fraction further amplified this effect.

3.3. Thermal Resistance

Increasing the volume fraction results in an increase in the convective coefficient and thermal dispersion, which are the main factors that reduce convective thermal resistance. The variation in the thermal resistance in this study is illustrated in Figure 7.

Figure 7 shows the differences in thermal resistance at concentrations of 0.5–1 vol. % and flow rates of 1–3 LPM. Higher flow rates represent lower thermal resistance; in other words, low resistance increases the convective coefficient and heat transfer rate. The increase in the number of NP also showed a downward trend, which reduced the thermal resistance. This emphasizes that the flow rate and volume fraction of the NP affect the performance of the HNF.

The observed trend of decreasing thermal resistance with increasing flow rate and volume fraction was consistent with the results of previous studies. For instance, Sohel *et al.* [31] reported that nanofluids containing Al_2O_3 exhibited 15.72% lower thermal resistance than conventional fluids. Similarly, Alnaqi [37] demonstrated that the addition of NP to the base fluid reduced the thermal resistance of the cooling system and improved the temperature uniformity at the surface, corroborating these results. However, the present study revealed a more pronounced reduction in thermal resistance, particularly at 1 vol. %, suggesting that the synergistic interaction between NP in the hybrid formulation further enhances the heat transfer efficiency. This discrepancy can be attributed to the differences in the NP dispersion and base fluid composition. These findings underscore the importance of optimizing the NP concentration and flow rate to achieve maximum thermal performance in HNF applications.

3.4. Thermal Effectiveness

Thermal effectiveness is important for understanding and evaluating the overall performance of HNF. The evaluation results can aid in the selection of the most effective parameters. **Figure 8** shows the thermal effectiveness of the HNF in the SHX with variations in the flow rate and NP amount. From the figure, it can be interpreted that a higher volume fraction indicates a higher thermal efficiency. At a flow rate of 1–3 LPM and a volume fraction of 0.5–1 vol. %, the effectiveness of HNF performance varies from 87 to 117%. The effectiveness of the HNF was calculated using Eq. (10), where the effectiveness value was based on the base temperature and fluid.

The thermal effectiveness of a cooling system is important for understanding its overall cooling performance. This aids in selecting the most effective system operating conditions [31]. The heat transfer benefits of Al_2O_3 nanofluids with 20:80 EG/W base fluid for all effective particle concentrations under laminar and turbulent flow conditions compared to 40:60 EG/W and 60:40 EG/W nanofluids for all particle concentrations [18]. The effectiveness is not always linear with the volume concentration [31]. Similarly, Ahmed *et al.* [38] reported that using TiO_2-water nanofluids with a concentration of 0.2% can increase the effectiveness of car radiators by 47% compared to concentrations of 0.1 and 0.3% and pure water. However, in the current study, it was observed that the higher the concentration, the higher the effectiveness. This may be due to the better performance of the HNF compared to that of the MNF and base fluids.

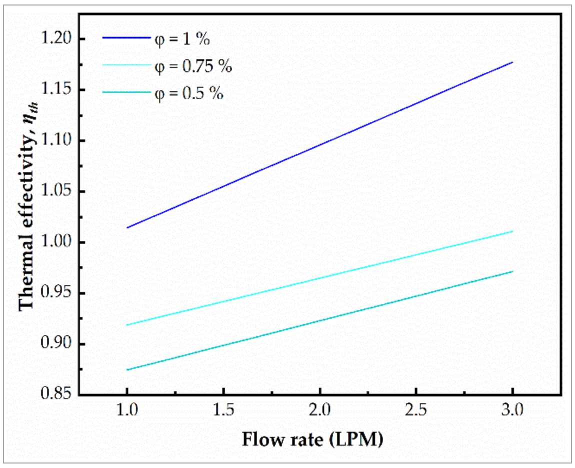

Figure 8. Influence of flow rate on the effectiveness of the SHX system at various nanofluid concentrations

3.5. Pressure Drop and Pumping Power

The pressure drop (*ΔP*) is an important parameter in the experiment because it affects the pumping power. During the pressure drop process, experiments were conducted at flow rates of 1, 2, and 3 LPM and different volume fractions. The pressure drops under both conditions are shown in **Figure 9**.

Figure 9 shows the pressure difference at volume fractions of 0.5–1 vol. % at 30 °C. In each volume fraction, *ΔP* is observed to increase at each flow rate; in other words, when each flow rate is increased, *ΔP* also increases. When the coolant passes through the SHX channel with small channel dimensions at both ends, a pressure drop occurs, which requires a greater pumping power. The increase in pumping power was calculated using Eq. (11), which shows the variation in the values with an increase in the flow rate and volume fraction of the gas. The much higher density of nanofluids is the main factor for increasing the pumping power compared with pure water. This finding indicates that higher flow rates improve the thermal performance, although they result in a slight increase in the pressure drop across the heat exchanger.

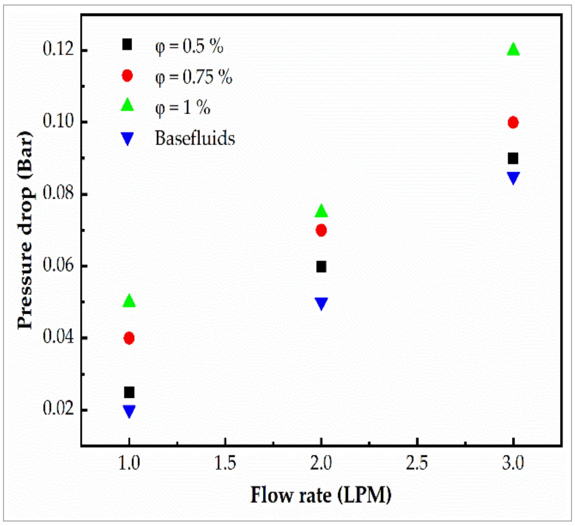

Figure 9. Influence of flow rate on the pressure drop in the SHX system at various nanofluid concentrations

The observed increasing trend of the pressure drop (ΔP) at higher flow rates and volume fractions was consistent with the findings of previous studies. Alnaqi [37] reported that an increase in the inlet velocity from 0.01 to 0.05 m/s enhanced the pumping power by 12.62 and 14.53 times, respectively. The current study showed comparable increases in ΔP, particularly at 1 V. %, indicating that the trade-off between thermal performance and pressure drop remains manageable. However, the hybrid nanofluid system (Al_2O_3–SiO_2) in this study showed a more gradual increase in the pressure drop than the single-component nanofluids. This is in line with the findings of Zawawi *et al.* [27], who emphasized that proper nanoparticle selection and stabilization techniques can mitigate excessive increases in viscosity. These results highlight the importance of balancing heat transfer enhancement with pumping power considerations, ensuring that hybrid nanofluids remain a viable alternative for SHX applications without significantly increasing operational costs.

4. Conclusion

In this study, the performance of a 20 Wp solar heat exchanger designed in a circular shape was tested using a Hybrid Nanofluid (HNF) Al_2O_3+SiO_2+EG/W (10:90) cooling fluid. The solar heat exchanger was experimentally tested at three flow rates: 1–3 LPM. Several important conclusions were drawn from this study. The HNF, as a solar heat exchanger coolant, experienced an increase in performance, with the highest heat transfer rate indicator of 56.07% compared with the base fluid. This increase in the heat transfer rate is consistent with the increase in the heat transfer coefficient, where the flow rate and volume fraction affect the increase in the HNF performance. The higher the flow rate, the higher the heat transfer rate, as well as the addition of nanoparticles, which also increases the heat transfer rate in SHX. The effectiveness of the HNF compared to that of the base fluid increased by ±117%, even though there was a slight increase in the pump power.

Acknowledgments

We would like to thank Sekolah Tinggi Teknologi Wastukancana for providing laboratory facilities and the opportunity to conduct this research. We would also like to thank Universitas Buana Perjuangan for their cooperation and help in providing testing equipment for this research.

Authors' Declaration

Authors' contributions and responsibilities - The authors made substantial contributions to the conception and design of the study. The authors took responsibility for data analysis, interpretation, and discussion of results. The authors read and approved the final manuscript.

Funding – We thank the Directorate of Research and Community Service and Directorate General of Research and Development of the Ministry of Research, Technology, and Higher Education of the Republic of Indonesia for funding this research through the Regular Fundamental Research program in 2024 with Contract Numbers 778/PP/STT-WKN/PWK/VI/2024 and 106/SP2H/RT-MONO/LL4/2024.

Availability of data and materials - All data is available from the authors.

Competing interests - The authors declare no competing interests.

Additional information – No additional information from the authors.

References

[1] A. Ibrahim, M. Y. Othman, M. H. Ruslan, S. Mat, and K. Sopian, "Recent advances in flat plate photovoltaic/thermal (PV/T) solar collectors," *Renewable and Sustainable Energy Reviews*, vol. 15, no. 1, pp. 352–365, Jan. 2011, doi: 10.1016/j.rser.2010.09.024.

[2] M. Ortiz, H. Barsun, H. He, P. Vorobieff, and A. Mammoli, "Modeling of a solar-assisted HVAC system with thermal storage," *Energy and Buildings*, vol. 42, no. 4, pp. 500–509, Apr. 2010, doi: 10.1016/j.enbuild.2009.10.019.

[3] J. Yoon *et al.*, "Flexible concentrator photovoltaics based on microscale silicon solar cells embedded in luminescent waveguides," *Nature Communications*, vol. 2, no. 1, p. 343, Jun. 2011, doi: 10.1038/ncomms1318.

[4] S. D. Prasetyo, E. P. Budiana, A. R. Prabowo, and Z. Arifin, “Modeling Finned Thermal Collector Construction Nanofluid-based Al2O3 to Enhance Photovoltaic Performance,” *Civil Engineering Journal*, vol. 9, no. 12, pp. 2989–3007, Dec. 2023, doi: 10.28991/CEJ-2023-09-12-03.

[5] B. J. Huang *et al.*, “Solar cell junction temperature measurement of PV module,” *Solar Energy*, vol. 85, no. 2, pp. 388–392, Feb. 2011, doi: 10.1016/j.solener.2010.11.006.

[6] H. G. Teo, P. S. Lee, and M. N. A. Hawlader, “An active cooling system for photovoltaic modules,” *Applied Energy*, vol. 90, no. 1, pp. 309–315, Feb. 2012, doi: 10.1016/j.apenergy.2011.01.017.

[7] M. S. Hossain, A. K. Pandey, J. Selvaraj, N. A. Rahim, M. M. Islam, and V. V. Tyagi, “Two side serpentine flow based photovoltaic-thermal-phase change materials (PVT-PCM) system: Energy, exergy and economic analysis,” *Renewable Energy*, vol. 136, pp. 1320–1336, Jun. 2019, doi: 10.1016/j.renene.2018.10.097.

[8] A. B. Al-Aasam, A. Ibrahim, K. Sopian, B. Abdulsahib M, and M. Dayer, “Nanofluid-based photovoltaic thermal solar collector with nanoparticle-enhanced phase change material (Nano-PCM) and twisted absorber tubes,” *Case Studies in Thermal Engineering*, vol. 49, p. 103299, Sep. 2023, doi: 10.1016/j.csite.2023.103299.

[9] E. Ebrahimnia-Bajestan, M. Charjouei Moghadam, H. Niazmand, W. Daungthongsuk, and S. Wongwises, “Experimental and numerical investigation of nanofluids heat transfer characteristics for application in solar heat exchangers,” *International Journal of Heat and Mass Transfer*, vol. 92, pp. 1041–1052, Jan. 2016, doi: 10.1016/j.ijheatmasstransfer.2015.08.107.

[10] M. A. Fikri *et al.*, “Characteristic of TiO2-SiO2 Nanofluid With Water/Ethylene Glycol Mixture for Solar Application,” *Journal of Advanced Research in Fluid Mechanics and Thermal Sciences*, vol. 81, no. 2, pp. 1–13, Mar. 2021, doi: 10.37934/arfmts.81.2.113.

[11] H. Adun *et al.*, “Synthesis and Application of Ternary Nanofluid for Photovoltaic-Thermal System: Comparative Analysis of Energy and Exergy Performance with Single and Hybrid Nanofluids,” *Energies*, vol. 14, no. 15, p. 4434, Jul. 2021, doi: 10.3390/en14154434.

[12] M. Hemmat Esfe *et al.*, “Thermal conductivity of Cu/TiO2–water/EG hybrid nanofluid: Experimental data and modeling using artificial neural network and correlation,” *International Communications in Heat and Mass Transfer*, vol. 66, pp. 100–104, Aug. 2015, doi: 10.1016/j.icheatmasstransfer.2015.05.014.

[13] F. Benedict *et al.*, “Thermal Performance of Hybrid-Inspired Coolant for Radiator Application,” *Nanomaterials*, vol. 10, no. 6, p. 1100, Jun. 2020, doi: 10.3390/nano10061100.

[14] A. Lenert and E. N. Wang, “Optimization of nanofluid volumetric receivers for solar thermal energy conversion,” *Solar Energy*, vol. 86, no. 1, pp. 253–265, Jan. 2012, doi: 10.1016/j.solener.2011.09.029.

[15] A. H. A. Al-Waeli, K. Sopian, M. T. Chaichan, H. A. Kazem, H. A. Hasan, and A. N. Al-Shamani, “An experimental investigation of SiC nanofluid as a base-fluid for a photovoltaic thermal PV/T system,” *Energy Conversion and Management*, vol. 142, pp. 547–558, Jun. 2017, doi: 10.1016/j.enconman.2017.03.076.

[16] T. K. Murtadha, A. A. dil Hussein, A. A. H. Alalwany, S. S. Alrwashdeh, and A. M. Al-Falahat, “Improving the cooling performance of photovoltaic panels by using two passes circulation of titanium dioxide nanofluid,” *Case Studies in Thermal Engineering*, vol. 36, p. 102191, Aug. 2022, doi: 10.1016/j.csite.2022.102191.

[17] S. M. Peyghambarzadeh, S. H. Hashemabadi, M. S. Jamnani, and S. M. Hoseini, “Improving the cooling performance of automobile radiator with Al2O3/water nanofluid,” *Applied Thermal Engineering*, vol. 31, no. 10, pp. 1833–1838, Jul. 2011, doi: 10.1016/j.applthermaleng.2011.02.029.

[18] L. Syam Sundar, E. Venkata Ramana, M. K. Singh, and A. C. M. Sousa, “Thermal conductivity and viscosity of stabilized ethylene glycol and water mixture Al2O3 nanofluids for heat transfer applications: An experimental study,” *International Communications in Heat and Mass Transfer*, vol. 56, pp. 86–95, Aug. 2014, doi: 10.1016/j.icheatmasstransfer.2014.06.009.

[19] R. S. Vajjha and D. K. Das, “Experimental determination of thermal conductivity of three nanofluids and development of new correlations,” *International Journal of Heat and Mass Transfer*, vol. 52, no. 21–22, pp. 4675–4682, Oct. 2009, doi:

10.1016/j.ijheatmasstransfer.2009.06.027.

[20] M. Hemmat Esfe, M. R. H. Ahangar, D. Toghraie, M. H. Hajmohammad, H. Rostamian, and H. Tourang, "Designing artificial neural network on thermal conductivity of Al2O3–water–EG (60–40 %) nanofluid using experimental data," *Journal of Thermal Analysis and Calorimetry*, vol. 126, no. 2, pp. 837–843, Nov. 2016, doi: 10.1007/s10973-016-5469-8.

[21] Mohd Amiruddin Fikri, Wan Mohd Faizal, Hasyiya Karimah Adli, Rizalman Mamat, Wan Hamzah Azmi, and Anwar Ilmar Ramadhan, "Experimental Study on Thermo-Physical Properties of TiO2-SiO2 Nanofluids (70:30) in Water/Ethylene Glycol Mixture," *Journal of Advanced Research in Fluid Mechanics and Thermal Sciences*, vol. 108, no. 2, pp. 200–214, Oct. 2023, doi: 10.37934/arfmts.108.2.200214.

[22] W. H. Azmi, K. Abdul Hamid, A. I. Ramadhan, and A. I. M. Shaiful, "Thermal hydraulic performance for hybrid composition ratio of TiO2–SiO2 nanofluids in a tube with wire coil inserts," *Case Studies in Thermal Engineering*, vol. 25, p. 100899, Jun. 2021, doi: 10.1016/j.csite.2021.100899.

[23] A. I. Ramadhan and W. H. Azmi, "The effect of nanoparticles composition ratio on dynamic viscosity of Al2O3-TiO2-SiO2 nanofluids," *Materials Today: Proceedings*, vol. 48, pp. 1920–1923, 2022, doi: 10.1016/j.matpr.2021.09.450.

[24] A. I. Ramadhan, W. H. Azmi, R. Mamat, E. Diniardi, and T. Y. Hendrawati, "Experimental Investigation of Cooling Performance in Automotive Radiator using Al2O3-TiO2-SiO2 Nanofluids," *Automotive Experiences*, vol. 5, no. 1, pp. 28–39, Nov. 2021, doi: 10.31603/ae.6111.

[25] ASHRAE Handbook, *Fundamentals*. American Society of Heating, Refrigeration and Air-Conditioning Engineers, 2009.

[26] S. Akilu, A. T. Baheta, K. Kadirgama, E. Padmanabhan, and K. V. Sharma, "Viscosity, electrical and thermal conductivities of ethylene and propylene glycol-based β-SiC nanofluids," *Journal of Molecular Liquids*, vol. 284, pp. 780–792, Jun. 2019, doi: 10.1016/j.molliq.2019.03.159.

[27] N. N. M. Zawawi, W. H. Azmi, M. Z. Sharif, and G. Najafi, "Experimental investigation on stability and thermo-physical properties of Al2O3–SiO2/PAG nanolubricants with different nanoparticle ratios," *Journal of Thermal Analysis and Calorimetry*, vol. 135, no. 2, pp. 1243–1255, Jan. 2019, doi: 10.1007/s10973-018-7670-4.

[28] B. C. Pak and Y. I. Cho, "Hydrodynamic and heat transfer study of dispersed fluids with submicron metallic oxide particles," *Experimental Heat Transfer*, vol. 11, no. 2, pp. 151–170, Apr. 1998, doi: 10.1080/08916159808946559.

[29] E. W. J. Mardles, "Viscosity of Suspensions and the Einstein Equation," *Nature*, vol. 145, no. 3686, pp. 970–970, Jun. 1940, doi: 10.1038/145970a0.

[30] R. L. Hamilton and O. K. Crosser, "Thermal Conductivity of Heterogeneous Two-Component Systems," *Industrial & Engineering Chemistry Fundamentals*, vol. 1, no. 3, pp. 187–191, Aug. 1962, doi: 10.1021/i160003a005.

[31] M. R. Sohel, S. S. Khaleduzzaman, R. Saidur, A. Hepbasli, M. F. M. Sabri, and I. M. Mahbubul, "An experimental investigation of heat transfer enhancement of a minichannel heat sink using Al2O3–H2O nanofluid," *International Journal of Heat and Mass Transfer*, vol. 74, pp. 164–172, Jul. 2014, doi: 10.1016/j.ijheatmasstransfer.2014.03.010.

[32] A. T. Wijayanta, I. Yaningsih, M. Aziz, T. Miyazaki, and S. Koyama, "Double-sided delta-wing tape inserts to enhance convective heat transfer and fluid flow characteristics of a double-pipe heat exchanger," *Applied Thermal Engineering*, vol. 145, pp. 27–37, Dec. 2018, doi: 10.1016/j.applthermaleng.2018.09.009.

[33] S. Khalid, I. Zakaria, W. H. Azmi, and W. A. N. W. Mohamed, "Thermal–electrical–hydraulic properties of Al2O3–SiO2 hybrid nanofluids for advanced PEM fuel cell thermal management," *Journal of Thermal Analysis and Calorimetry*, vol. 143, no. 2, pp. 1555–1567, Jan. 2021, doi: 10.1007/s10973-020-09695-8.

[34] G. M. Moldoveanu, G. Huminic, A. A. Minea, and A. Huminic, "Experimental study on thermal conductivity of stabilized Al2O3 and SiO2 nanofluids and their hybrid," *International Journal of Heat and Mass Transfer*, vol. 127, pp. 450–457, Dec. 2018, doi: 10.1016/j.ijheatmasstransfer.2018.07.024.

[35] P. Kanti, K. V. Sharma, C. G. Ramachandra, and B. Panitapu, "Stability and thermophysical

properties of fly ash nanofluid for heat transfer applications," *Heat Transfer*, vol. 49, no. 8, pp. 4722–4737, Dec. 2020, doi: 10.1002/htj.21849.

[36] P. Keblinski, S. . Phillpot, S. U. . Choi, and J. . Eastman, "Mechanisms of heat flow in suspensions of nano-sized particles (nanofluids)," *International Journal of Heat and Mass Transfer*, vol. 45, no. 4, pp. 855–863, Feb. 2002, doi: 10.1016/S0017-9310(01)00175-2.

[37] A. A. Alnaqi, "Numerical analysis of pressure drop and heat transfer of a Non-Newtonian nanofluids in a Li-ion battery thermal management system (BTMS) using bionic geometries," *Journal of Energy Storage*, vol. 45, p. 103670, Jan. 2022, doi: 10.1016/j.est.2021.103670.

[38] S. A. Ahmed, M. Ozkaymak, A. Sözen, T. Menlik, and A. Fahed, "Improving car radiator performance by using TiO2-water nanofluid," *Engineering Science and Technology, an International Journal*, vol. 21, no. 5, pp. 996–1005, Oct. 2018, doi: 10.1016/j.jestch.2018.07.008.